electronics

MDPI

Article

A Forward-Backward Iterative Procedure for Improving the Resolution of Resonant Microwave Sensors

Giovanni Buonanno [1,*], Adriana Brancaccio [1], Sandra Costanzo [2,3,4] and Raffaele Solimene [1,5,6]

[1] Department of Engineering, University of Campania, 81031 Aversa, Italy; adriana.brancaccio@unicampania.it (A.B.); raffaele.solimene@unicampania.it (R.S.)
[2] Department of Computer Science, Modelling, Electronic and Systems (DIMES), University of Calabria, 87036 Rende, Italy; costanzo@dimes.unical.it
[3] Institute for Electromagnetic Sensing of the Environment (IREA), National Research Council (CNR), 80124 Naples, Italy
[4] National Inter-University Research Center on the Interactions between Electromagnetic Fields and Biosystems (ICEmB), 16145 Genoa, Italy
[5] National Inter-University Consortium for Telecommunications (CNIT), 43124 Parma, Italy
[6] Department of Electrical Engineering, Indian Institute of Technology Madras, Chennai 600036, India
* Correspondence: giovanni.buonanno@unicampania.it

Abstract: This paper sets out a method for improving the resolution of resonant microwave sensors. Usually, the frequency response of these devices is associated with a low quality factor, and consequently with a low resolution in terms of tracking capacity of the resonance frequency shift. Furthermore, since only a finite number of samples can be acquired during the measurement process, the "true" resonance frequency may not be included in the set of acquired data. In order to have an accurate estimate of the resonance frequency, high performance systems with very fine frequency sampling are thus required. To limit these drawbacks, an iterative algorithm is presented which aims to refine the response of resonant microwave sensors by means of a suitable post-processing. The algorithm evaluation is first carried out on synthetic data, and then applied on experimental data referring to a practical scenario, which is inherent to return loss measurements performed by a microwave patch antenna immersed in a water-glucose solution with different concentrations.

Keywords: microwaves resonant sensors; blood glucose monitoring; signal processing

Citation: Buonanno, G.; Brancaccio, A.; Costanzo, S.; Solimene, R. A Forward-Backward Iterative Procedure for Improving the Resolution of Resonant Microwave Sensors. *Electronics* **2021**, *10*, 2930. https://doi.org/10.3390/electronics10232930

Academic Editor: Jung-Chih Chiao

Received: 31 October 2021
Accepted: 22 November 2021
Published: 26 November 2021

1. Introduction

Nowadays, microwave sensors are found in a variety of contexts, as their field of application is extremely broad. They have very interesting peculiarities, and among them microwave (resonant) sensors based on resonant devices are particularly attractive, as their frequency response is highly sensitive to the characteristics of the investigated medium in which they are inserted [1]. For example, referring to biomedical applications, in [2], the design of a resonant microwave sensor for applications related to blood glucose monitoring is proposed, showing that, in order to obtain a sensor suitable to provide an accurate estimation of the glucose concentration level, it is necessary to take into account the variations of both the real and the imaginary part of the complex permittivity of the medium under investigation as a function of frequency, yet discussed in [3]. In [4], still considering the problem of blood glucose monitoring, a portable prototype of a planar microwave sensor is shown, consisting of four distinct hexagonal-shaped complementary split ring resonators. Instead, in [5], microwave and millimeter wave dielectric spectroscopy performed at the cellular and molecular level is discussed, in the context of early cancer diagnostics.

In [6], a planar two-dimensional inductor–capacitor circuit is instead used as a resonant sensor for monitoring of temperature, humidity, and pressure. In [7], a chain of complementary split-ring resonators is used both for the measurement of dielectric constants as well as for faults detection. Resonant sensors are also used for angular displacement

and velocity measurements in satellite applications [8], for detection of acetone vapour [9], and for the characterisation of aqueous solutions [10].

An important class of microwave resonant sensors are the frequency-variation sensors, for which the behavior of the frequency response depends on the variations of the *measurand* [1]. Typically, such sensors can have a low quality factor, which results in a relatively much wider than ideal frequency response pattern. This in turn results in a low resolution, and therefore in a low tracking ability of the resonance frequency shift [11]. This problem can be addressed from the circuit point of view, by means of some active microwave device which allows an increase in the quality factor of sensors [11,12]. However, another important aspect to be considered is related to the fact that the frequency response samples, acquired by the measurement instrumentation, represent a discrete set with finite extension, so there is a very high probability that the sample associated with the resonance frequency will not be captured correctly.

In order to limit the above drawbacks, an iterative algorithm is proposed in this work which leads to post-process the acquired samples of the frequency response, in order to significantly increase the quality factor and therefore achieve a more accurate estimate of the resonance frequency. This algorithm has high performance even starting from a relatively very low number of acquired samples of the sensor response within a frequency band with a high extension. In this way, even unsophisticated measuring equipment can be exploited.

An appropriate performance analysis of this algorithm is first carried out using synthetic data; then, the proposed method is tested on measured data collected by a microstrip patch antenna immersed in a water-glucose solution, which represents a simplified case in the context of a blood glucose monitoring problem.

2. Iterative Method to Improve the Resolution of Resonant Sensors

The algorithm presented in this section is based on an iterative procedure inspired by the Papoulis–Gerchberg algorithm [13,14]. However, while the objective of the Papoulis–Gerchberg algorithm is to estimate the Fourier transform of a signal starting from its truncated version, the aim of the proposed method is to progressively narrow the sensor response in such a way to reach, from the starting signal, a *sinc* function with a very narrow main lobe, whose point of maxima coincides with the resonance frequency.

Let us consider a signal as that depicted in Figure 1a, which is representative of the sensor return loss measured between the frequencies f_{min} and f_{MAX}, namely [15]:

$$RL(f) = -20 \log_{10} |\Gamma(f)|. \quad (1)$$

The function $\Gamma(f)$ into Equation (1) represents the reflection coefficient at the microwave sensor input. An interesting aspect to be remarked is that here we are going to work with values expressed in dB for the magnitude of the reflection coefficients (regardless of the presence of the minus sign in the definition), and thence the computation of the Fourier transform of the return loss is as equivalent to a "sort" of complex cepstrum [16] of the inverse Fourier transformation of $|\Gamma(f)|$.

A brief consideration is relative to the presence of noise. In this paper, we assume the signal is smooth enough so that the noise can be considered almost full negligible. However, in practice this cannot always be ensured, and thence the size of the signal-to-noise ratio (SNR) must be taken into account in order to be able to adequately process the return loss. However, one solution is to carry out more acquisitions of the return loss, and then to perform a sample average of these acquisitions, in order to significantly improve the SNR, without distorting the "true" signal.

Now, let us move on to introduce the various steps that make up the algorithm we intend to propose. Assume that $RL(f_{min}) < RL(f_{MAX})$ (similar arguments hold true when $RL(f_{min}) > RL(f_{MAX})$) and that the curve has a single maximum in $[f_{min}, f_{MAX}]$. The algorithm consists of the following steps:

1. Determine the frequency value $\tilde{f}$, such that $RL(\tilde{f}) = RL(f_{MAX})$ (refer to Figure 1b).

2. Define (refer to Figure 1c):

$$\widetilde{RL}(f) = \begin{cases} RL(\widetilde{f}) & f_{min} \le f \le \widetilde{f} \\ RL(f), & \widetilde{f} \le f \le f_{MAX} \end{cases}. \tag{2}$$

3. Shift $\widetilde{RL}(f)$ down by a quantity equal to $RL(\widetilde{f}) = RL(f_{MAX})$, so that now the "new" return loss, $\overline{RL}(f)$, is as shown in Figure 1d, i.e., it is bereft of end points.
4. Set up a threshold $0 < \alpha < 1$ for $\overline{RL}(f)/\max\{\overline{RL}(f)\}$ in order to identify the two values $\overline{f}_{min}$ and $\overline{f}_{MAX}$ such that (Figure 1d):

$$\frac{\overline{RL}(\overline{f}_{min})}{\max\{\overline{RL}(f)\}} = \frac{\overline{RL}(\overline{f}_{MAX})}{\max\{\overline{RL}(f)\}} = \alpha \tag{3}$$

thus obtaining the narrower frequency observation interval $[\overline{f}_{min}, \overline{f}_{MAX}]$.
5. Compute the inverse Fourier transform of $\overline{RL}(f)$ (for $\nu \in [\nu_{min}, \nu_{MAX}]$):

$$rl(\nu) = \int_{f_{min}}^{f_{MAX}} \overline{RL}(f)\, e^{j2\pi\nu f}\, df \tag{4}$$

in order to obtain the complex function of Figure 2a. As seen, $rl(\nu)$ exhibits an almost linear unwrapped phase $\phi(\nu) = \angle rl(\nu)$ (bottom panel of Figure 2a) in correspondence of the main lobe (top panel of Figure 2a), which actually encodes information about the peak of the resonance frequency.
6. Set up a threshold $0 < \beta < 1$.
7. Determine the two values $\tilde{\nu}_{min}$ and $\tilde{\nu}_{MAX}$ for $|rl(\nu)|/\max\{|rl(\nu)|\}$ in such a way (Figure 2a):

$$\frac{|rl(\tilde{\nu}_{min})|}{\max\{|rl(\nu)|\}} = \frac{|rl(\tilde{\nu}_{MAX})|}{\max\{|rl(\nu)|\}} = \beta \tag{5}$$

in order to pick out the interval $[\tilde{\nu}_{min}, \tilde{\nu}_{MAX}]$ inside of which there is a greater reliability of the phase information.
8. Replace $|rl(\nu)|$ with a unitary rectangular window supported over $[\tilde{\nu}_{min}, \tilde{\nu}_{MAX}]$, whereas the actual phase is instead retained. Consequently, the new signal $\widehat{rl}(\nu) = e^{j\phi(\nu)}\ \forall\, \nu \in [\tilde{\nu}_{min}, \tilde{\nu}_{MAX}]$ (and equal to zero elsewhere) is given by the curves in Figure 2b.
9. Determine the magnitude of the Fourier transform of $\widehat{rl}(\nu)$ (for $f \in [\overline{f}_{min}, \overline{f}_{MAX}]$):

$$\widehat{RL}(f) = \left| \int_{\tilde{\nu}_{min}}^{\tilde{\nu}_{MAX}} e^{j\phi(\nu)}\, e^{-j2\pi\nu f}\, d\nu \right| \tag{6}$$

which returns a new return loss (blue curve of Figure 3) that is narrower than the original one (of Figure 1a). By calculating the new return loss only in the interval $[\overline{f}_{min}, \overline{f}_{MAX}]$, we are doing a sort of magnification in the region in which the resonance frequency is assumed to be.
10. Compute the inverse Fourier transform of the squared current return loss (i.e., of the square of the blue curve of Figure 3):

$$rl(\nu) = \int_{\overline{f}_{min}}^{\overline{f}_{MAX}} \widehat{RL}^2(f)\, e^{j2\pi\nu f}\, df \tag{7}$$

so that the magnitude and the unwrapped phase of $rl(\nu)$ are now like the blue curves sketched in the top and bottom panels of Figure 4a, respectively. It should be noted that here we are implicitly assuming that $\widehat{RL}(f)$ is nonzero only in $[\overline{f}_{min}, \overline{f}_{MAX}]$. By comparing the previous and the current version of $rl(\nu)$, now the magnitude main lobe is wider (this is due to squaring $\widehat{RL}(f)$ in (7)) and the region where the instantaneous phase is linear wider. In fact, in correspondence with the threshold β, two new values of ν are identified, i.e., $|rl(\widehat{\nu}_{min})|/\max\{rl(\nu)\} = |rl(\widehat{\nu}_{MAX})|/\max\{rl(\nu)\} = \beta$ such

that $\hat{\nu}_{min} < \tilde{\nu}_{min}$ and $\hat{\nu}_{MAX} > \tilde{\nu}_{MAX}$. By way of example, if from this step one returned to step 7 and the same step 7 were performed together with steps 8 and 9, the new return loss would be given by the red curve of Figure 5.

11. Repeat points 7 to 10 until the function $rl(\nu)$ is such that $|rl(\nu)|/\max\{|rl(\nu)|\} \geq \beta \; \forall \; \nu \in [\nu_{min}, \nu_{MAX}]$ and, in the end, compute the final return loss by Equation (6), whose point of maxima gives the estimated resonance frequency. For greater clarity, it is worth remembering that ν_{min} and ν_{MAX} are the extremes of the whole observation interval of the function $rl(\nu)$.

For a better understanding of the algorithm process, a flowchart description is reported in Figure 6.

It is worthwhile to remark that the different Fourier transformations involved in the previous steps are actually achieved by the discrete time Fourier transform (DTFT) procedure, which allows to control in a very flexible way both the number and the positioning (e.g., periodic or aperiodic) of the observation points of the various transformations in specific intervals. This entails that even starting with N_f number of points, which correspond to the frequencies actually collected by the sensor, the number of points in the ν-domain, N_ν, and subsequently in the f-domain, $\hat{N}_f$, can be chosen on the basis of convenience. This implies a very advantageous practical aspect, since it may happen that the frequency step allowed by the acquisition system is not sufficiently fine for the actual resonance peak to be captured well. The proposed method, on the other hand, allows one to reduce the difference between the frequencies of adjacent samples, and therefore a better estimate of the resonance frequency is expected.

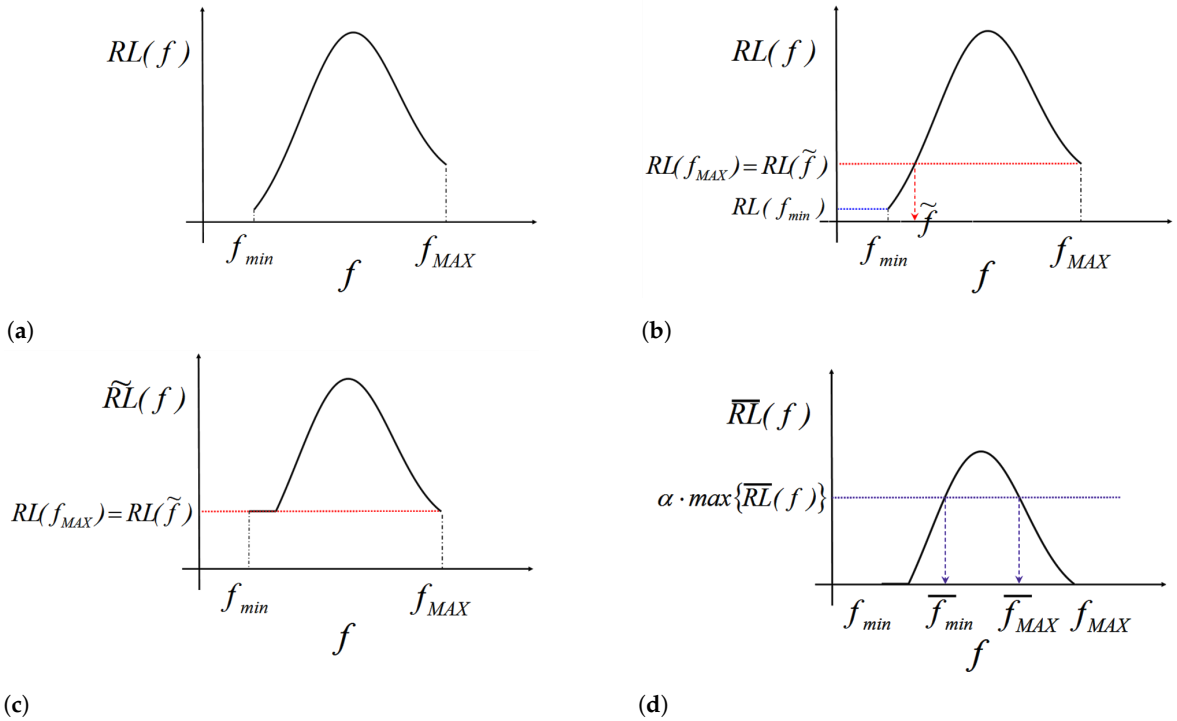

Figure 1. Illustrating steps 1 to 4. (**a**) Signal mimicking the return loss of a resonant sensor. (**b**) Identification of the frequency value $\tilde{f}$. (**c**) Removing all values of the return loss below $RL(\tilde{f})$. (**d**) Identification of the frequency values $\overline{f}_{min}$ and $\overline{f}_{MAX}$.

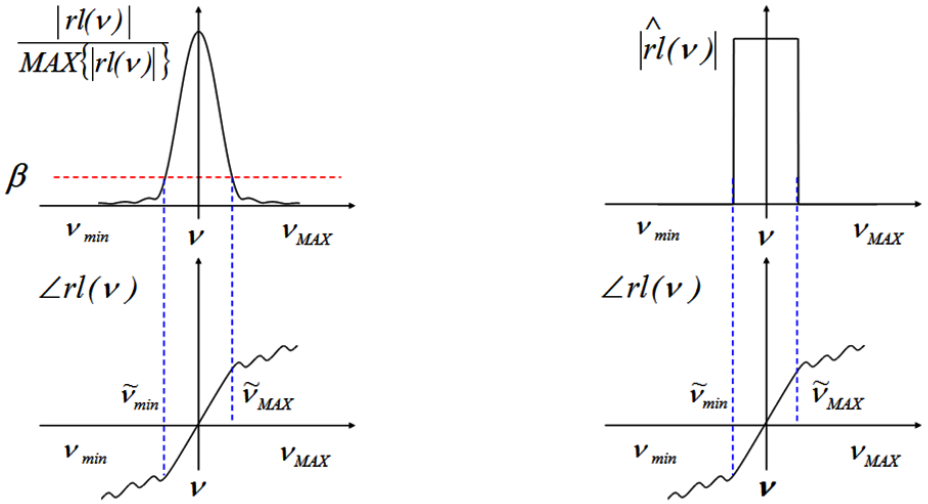

(**a**) (**b**)

Figure 2. Illustrating steps 5 to 8. (**a**) magnitude and phase of $rl(\nu)$; (**b**) magnitude and phase of $\widehat{rl}(\nu)$.

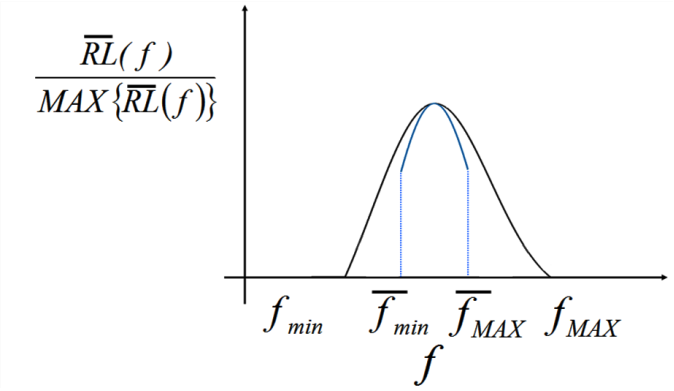

Figure 3. After step 9, $RL(f)$, computed only in $[\overline{f}_{min}, \overline{f}_{MAX}]$, is narrowed (blue curve) as compared to the initial one (black curve).

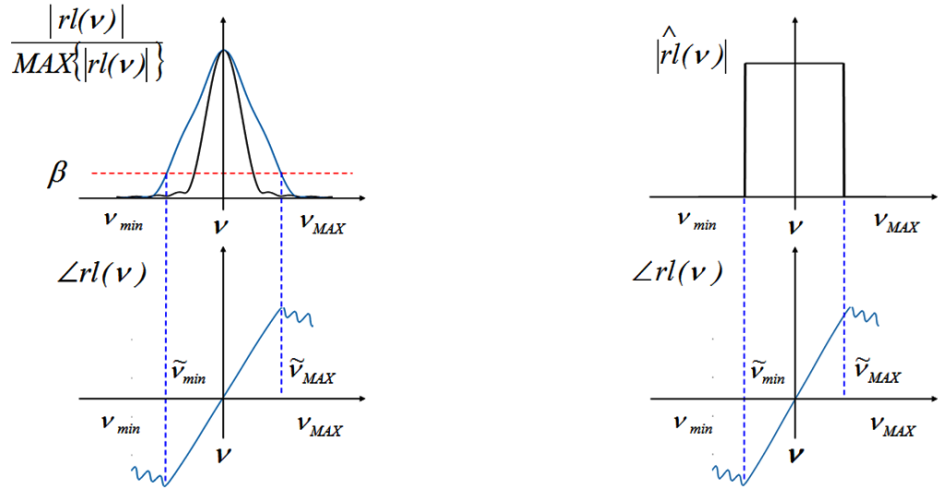

(**a**) (**b**)

Figure 4. Step 10. (**a**) comparing the obtained $rl(\nu)$ (blue lines) and the previous one (black line). (**b**) Next windowing step over the corresponding larger interval in the ν-domain.

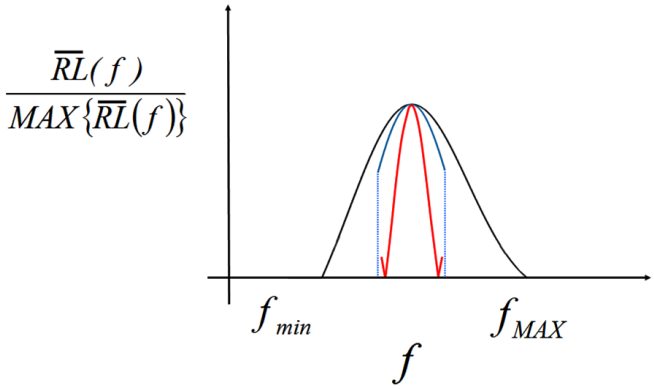

Figure 5. Comparison between the new return loss (red curve) obtained from the function $\widehat{rl}(\nu)$ of Figure 4b with the previous ones.

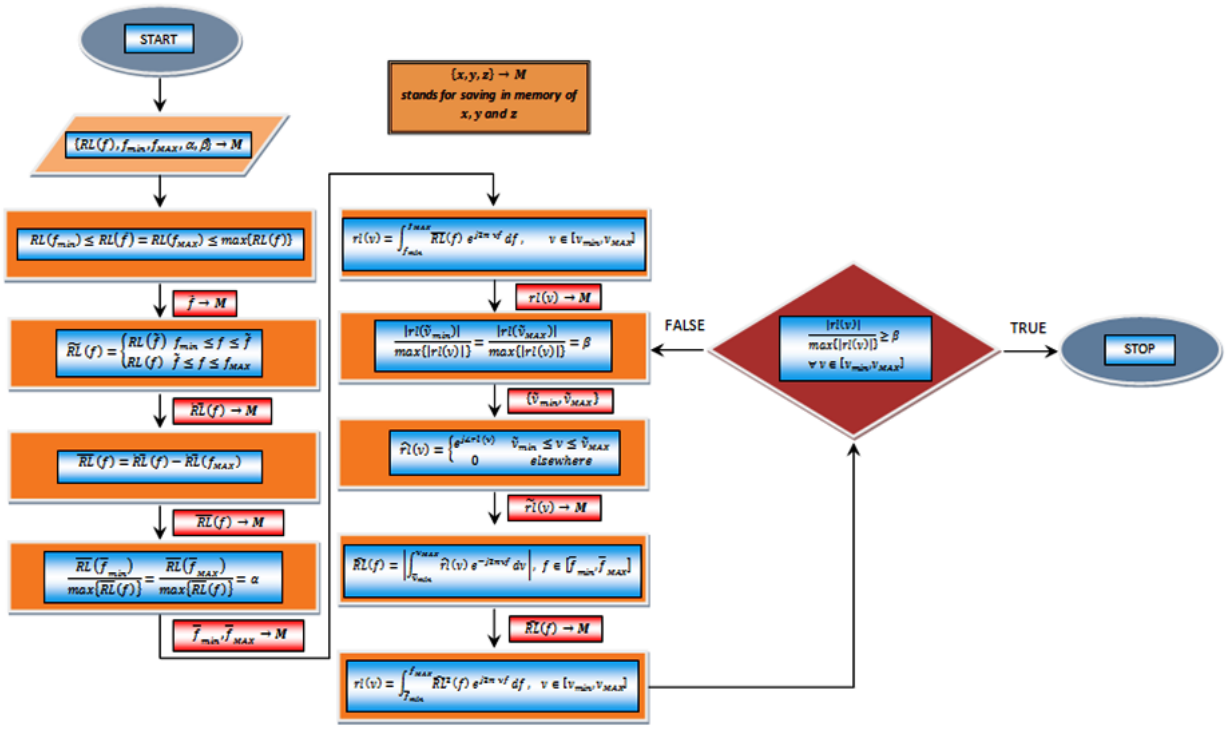

Figure 6. Flowchart describing the proposed algorithm.

Now, before moving on to the assessment of the algorithm under consideration, it is worth investigating further some practical aspects in relation to how α is determined and the implementation aspects of the Fourier transforms related to the functions $rl(\nu)$ and $\widehat{RL}(f)$. In particular, Equation (3) would require that, strictly speaking, α be determined with respect to the maximum value of the return loss, which however is actually unknown in real scenarios. However, from a practical point of view, in reality α is calculated with respect to the maximum value of the acquired return loss, that is, $\max\{\overline{RL}(f)\}$ is the highest value among those acquired during the measurement process. As for computation of $rl(\nu)$ and $\widehat{RL}(f)$, Equation (4) is implemented by sampling in N_ν points of the interval $[\nu_{min}, \nu_{MAX}]$ the inverse DTFT of the acquired N_f points in $[f_{min}, f_{MAX}]$ of the initial return loss; Equation (6) is implemented by sampling in $\widehat{N}_f$ points of the interval $[\overline{f}_{min}, \overline{f}_{MAX}]$ the DTFT of the $rl(\nu)$ samples (of the total N_ν samples) that fall in $[\tilde{\nu}_{min}, \tilde{\nu}_{MAX}]$. Obviously, it is possible to change parameters N_ν, $\widehat{N}_f$, the positioning of the samples of $rl(\nu)$ and $\widehat{RL}(f)$ and also the thresholds α and β even during the execution of the algorithm, in order to

perform a kind of "dynamic" performance control. Furthermore, we choose to keep the extension of the temporal observation interval constant, thus fixing *ab initio* in the way that is explained below the values of ν_{min} and ν_{MAX}, even if, in general, the value of these parameters could also be changed while running the algorithm.

Another important consideration concerns the setting of the acquisition band, i.e., the choice of f_{min} and f_{MAX}. Due to the algorithm structure, in order to obtain an accurate estimate of the resonance frequency, it is required that f_{min} and f_{MAX} must be such that the "acquired" return loss has an increasing trend up to the point of maxima (or to the points of maxima in case of multiple acquired maximum values), inside $[f_{min}, f_{MAX}]$, and then after the same point is decreasing. Thence, during the acquisition stage, a simple procedure for analysing the trend of the initial return loss could also be set up in order to verify whether the above condition is satisfied.

Finally, the frequency and time steps should be also considered. In fact, if the various functions are sampled uniformly (which we assume below), then there is an initial frequency step given by $\Delta_f = (f_{MAX} - f_{min})/(N_f - 1)$ (assuming that any sampling errors on the part of the measurement system are negligible), a subsequent frequency step given by $\widehat{\Delta}_f = (\overline{f}_{MAX} - \overline{f}_{min})/(\widehat{N}_f - 1)$, and a time step given by $\Delta_t = (\nu_{MAX} - \nu_{min})/(N_\nu - 1)$, with $\nu_{min} = -\nu_{MAX} = -0.5/\Delta_f$.

In the following, the proposed algorithm is applied both to synthetic and experimental signals by resorting to the environment for numerical computation MATLAB [17].

3. Iterative Algorithm Application to Synthetic Data

In this section, we turn to check the presented algorithm by employing a simple signal that mimics the response of a resonant sensor. The main aim is to better clarify the key features of the method. To this end, we initially consider the following values for parameters: $N_f = 1001$, $N_\nu = 2^{12} = 4096$, $\widehat{N}_f = 4096$, $f_{min} = -f_{MAX} = -0.5$ GHz. From the values of the these parameters, it follows that the initial frequency step is equal to $\Delta_f = (f_{MAX} - f_{min})/(N_f - 1) = 1$ MHz and $\nu_{min} = -\nu_{MAX} = -0.5/\Delta_f = -0.5\,\mu$s. Note that, considering a frequency observation band centred with respect to $f = 0$, it means addressing the problem in base-band and thence, in general, it entails to estimate the frequency shift, f_{shift}, with respect to the midpoint frequency of a generic observation band. Consequently, the resonance frequency is simply given by the sum of the central frequency of the original band (of the band-pass signal) plus the frequency shift.

Now, let us consider a return loss in $[f_{min}, f_{MAX}] = [-0.5$ GHz, 0.5 GHz] given by the following relationship:

$$RL(f) = \begin{cases} 10 \times e^{-\frac{(f\ +\ 200.5\times10^6)^2}{2\left(0.07\times10^9\right)^2}} + 5 & f_{min} \le f \le -200.5 \times 10^6 \\ 10 \times e^{-\frac{(f\ +\ 200.5\times10^6)^2}{2\left(0.10\times10^9\right)^2}} + 5 & -200.5 \times 10^6 \le f \le f_{min} \end{cases} \quad (8)$$

i.e., the combination of two "half" Gaussian functions, both with maximum values equal to 15 and mean (point of maxima) equal to -200.5 MHz. However, the first one has a standard deviation of 70 MHz while the second one of 100 MHz. A curve of this type can be close to the actual frequency response of a resonant sensor. It is worth pointing out that, for how the values of the above parameters are set, the frequency -200.5 MHz is not included in the set of initial return loss points. Therefore, here we propose both to tighten the initial return loss and to more accurately identify the frequency shift.

Figure 7 shows the behavior of the percentage error, $PE = |(\overline{f_{shift}} - f_{shift})/f_{shift}| \times 100\%$, as a function of the two thresholds α and β, with $\overline{f_{shift}}$ and f_{shift} being the estimated and actual frequency shift (i.e., $f_{shift} = -200.50$ MHz), respectively. As can be seen, these thresholds have a relatively strong impact on PE values, being able to notice that they are non-linearly related to PE. In particular, it can be observed that for the considered cases, the minimum percentage error value is for $(\alpha, \beta) = (0.85, 0.05)$.

Figure 8 shows the results of applying the algorithm specifically in the case in which $(\alpha, \beta) = (0.85, 0.05)$. Figure 8a shows both the (normalised) initial return loss (blue curve), given by Equation (8), and the normalised one (red curve) obtained by applying steps 1 to 3 of the algorithm, which has no end points. The magnitudes of the (normalised) inverse DTFTs of these signals are reported in Figure 8b, which shows that they differ significantly from zero over a much smaller interval than the entire observation one $[\nu_{min}, \nu_{MAX}] = [-0.5, 0.5]$ µs. These are actually the parts that must be retained. Indeed, it is clear from Figure 8c that in this smaller interval the phase of $rl(\nu)$ shows a different slope as compared to the regions where the magnitude of $rl(\nu)/\max\{|rl(\nu)|\}$ is negligible. Therefore, this justifies why we focus on the main lobe of $rl(\nu)/\max\{|rl(\nu)|\}$. Furthermore, it should be noted that if the end points are removed, the function $rl(\nu)$ has a different behaviour than that relating to the case in which this removal is not performed, as can be clearly recognised by observing the blue and red curves of Figure 8b,c. In particular, by looking at the inset of Figure 8b, it can be seen that removing the end points allows for a larger interval $[\widetilde{\nu}_{min}, \widetilde{\nu}_{MAX}]$ (which is positive for narrowing the RL). In the end, Figure 8d shows the comparison between the initial return loss and the final return losses obtained at the end of the full application of the algorithm, although it must be taken into account that the blue dot sinc-like curve is relative to the case in which steps 1 to 3 are not applied to the initial return loss (blue curve of Figure 8a). In fact, although the final curves turns out to be much tighter than the initial ones; to the blue dot curve corresponds $PE \approx 9.23\%$ while to the red one corresponds $PE \approx 0.09\%$. Therefore, this shows that the removal of the end points turns out to be beneficial from a performance point of view.

Now, let us focus on the resolution capability of the algorithm under consideration. Here, we refer to the Rayleigh criterion for the diffraction limit to resolution, therefore going to verify if it is possible to distinguish two frequency shifts if their distance is at least equal to half the width of the main lobe of the "correct" final return loss. So, referring to the red curve of Figure 8d, we have that the width (beamwidth) of its main lobe is approximately equal to $BW = 2.01$ MHz. Consequently, for what is said above, let us now consider the case in which the initial return loss has an actual frequency shift equal to $f_{shift} + BW/2 \approx -199.50$ MHz (remember that $f_{shift} = -200.50$ MHz), that is, it is shifted to the right with respect to the blue curve of Figure 8a of $BW/2$ (refer to Figure 9a). As can be seen from Figure 9b, in which now the blue curve coincides with the red curve of Figure 8d whilst the red-dashed curve with the final return loss of the present case, the performance in terms of resolution is satisfactory, as the point of maxima of the above red dashed curve has a high correspondence with -199.50 MHz. In fact, even in this case the percentage error is $PE \approx 0.09\%$. Obviously, also in this case, it has been placed $(\alpha, \beta) = (0.85, 0.05)$, $N_f = 1001$, $N_\nu = \widehat{N}_f = 4096$.

Finally, it is worth asking about the performance behaviour of the algorithm in question when changing the number of initial points, N_f. To do this, let us consider Figure 10, which shows the trend of the percentage error as a function of N_f, again for $(\alpha, \beta) = (0.85, 0.05)$, $N_\nu = \widehat{N}_f = 4096$, and $f_{shift} = -200.50$ MHz. Looking at the figure, it can be seen that the number of samples of the initial return loss also impacts the performance in a non-linear way, even if higher values of N_f correspond, in a wide sense, to smaller values of PE. In fact, this can be confirmed by the negative slope of the linear regression straight line shown in red in the same figure. Furthermore, even if approximately between 600 and 900 samples the difference between the computed values of PE and the above linear regression straight line is relatively marked, compared with what is obtained for the other values of N_f, it is also true that the computed values of the percentage error after 600 samples starts to drop and then remain below 1%. However, it can also be observed that when N_f goes from 1001 to 101, the performance degradation is still small, as the percentage error does not exceed 2%.

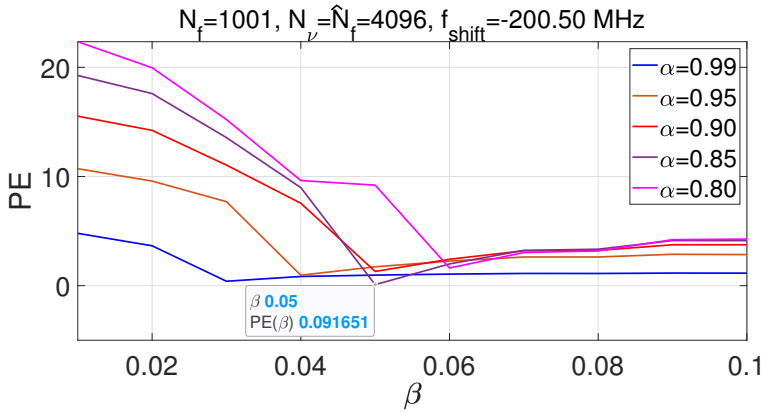

Figure 7. Percentage error as a function of α and β.

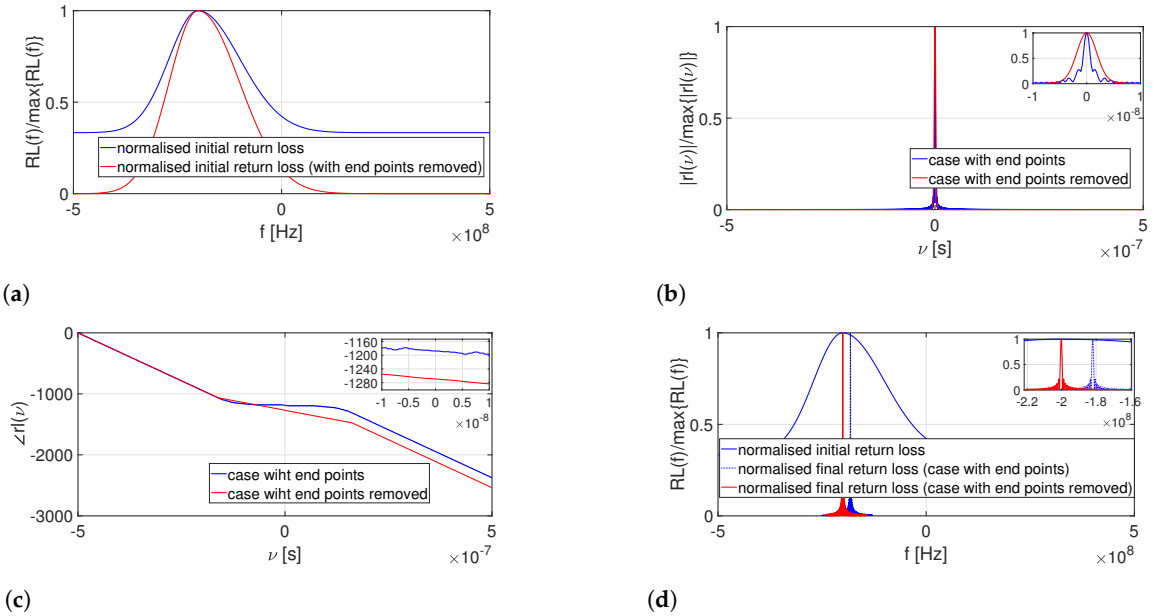

Figure 8. Application of the algorithm to the return loss given by Equation (8). (**a**) Normalised initial return loss (blue line) and its version (red line) after steps 1 to 3 have run. (**b**,**c**) Corresponding *rl*s. (**d**) Final outcome with (red line) and without (blue dotted line) running the first three steps. The parameters were set as follows: $N_f = 1001$, $N_\nu = \widehat{N}_f = 4096$, $(\alpha, \beta) = (0.85, 0.05)$, $f_{shift} = -200.50$ MHz.

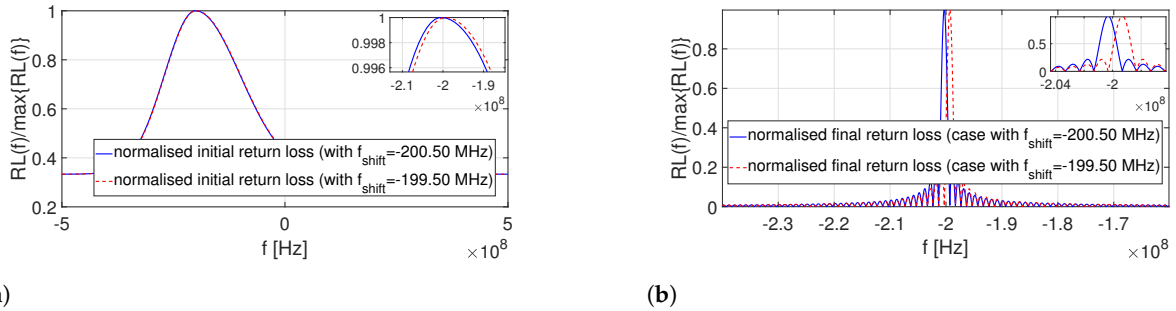

Figure 9. Evaluation of the resolution of the proposed algorithm. (**a**) Normalised initial return losses with points of maxima equal to -200.5 MHz (blue line) and -199.50 MHz (red line). (**b**) Corresponding final return losses. The other parameters were set as follows: $N_f = 1001$, $N_\nu = \widehat{N}_f = 4096$, $(\alpha, \beta) = (0.85, 0.05)$.

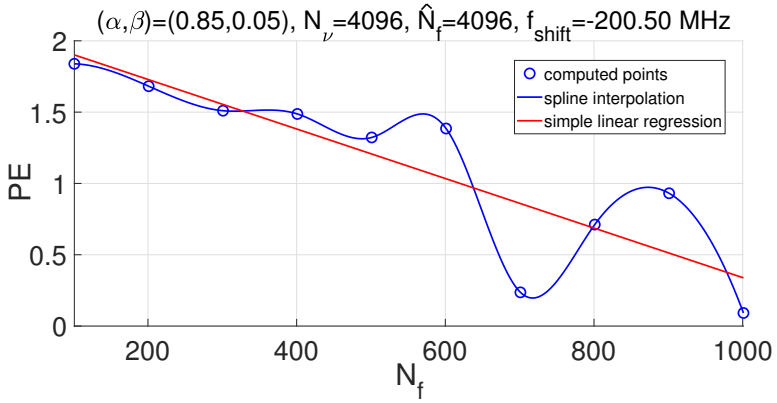

Figure 10. Percentage error as a function of the number of samples, N_f, of the initial return loss.

4. Iterative Algorithm Application to Experimental Data

In this section, the algorithm previously discussed is applied to return loss data captured by the resonant microwave sensor described in [2], in the context of blood glucose monitoring. This sensor consists of a standard inset-fed microstrip patch antenna working in the Industrial, Scientific, Medical (ISM) band around the frequency $f_0 = 2.4$ GHz. The substrate has a relative dielectric constant equal to $\varepsilon_r = 10$.

The accurate design of a typical microwave sensor able to capture dielectric variations of human body parameters should be performed by starting from a proper definition of a multilayer model for the human body portion assumed as the radiation medium. Specifically, an accurate body stratification should be assumed, by considering the proper behaviour of complex permittivity versus frequency (i.e., the dispersive behaviour) for each layer. The effectiveness of the dielectric models assumed for the various layers and the performance of the methods used to fit those models play a crucial role in the accuracy of the design process of the microwave sensor [2,3,18,19].

In this paper, without affecting the conceptual validity of the algorithm under investigation, we consider a simplified scenario that consists in estimating the resonance frequency of the sensor immersed in a water-glucose solution as the glucose concentration, GC, inside it varies. Consequently, consistent with the foregoing, for the design of the above sensor the properties of a water-glucose solution were first investigated, thus characterising the behaviour of its complex permittivity (the dielectric constant as well as the loss tangent) as a function of the concentration of glucose levels. Subsequently, data obtained from the above analysis were used to proceed to the actual design of the sensor through an optimisation performed using the Ansys software, in such a way as to have optimum matching conditions at the prescribed frequency $f_0 = 2.4$ GHz. In Figure 11, a photograph of the fabricated microwave sensor is reported, which is immersed into water-glucose solutions to perform reflection measurements at the Microwave Laboratory of University of Calabria.

Figure 12 shows the experimental (normalised) return loss measured for the water-glucose solution with different values of the glucose concentration where it can be clearly appreciated how the resonance frequency shifts with GC.

To run the sharpening algorithm, the data measured within the frequency band $[2, 3]$ GHz are first shifted at the band $[-0.5, 0.5]$ GHz. Accordingly, as mentioned above, this implies that the resonance frequency estimated by the algorithm returns the frequency shift, $\overline{f_{shift}}$, with respect to the middle frequency of the measurement band, i.e., with respect to 2.5 GHz. For each measured curve, the algorithm is run for different values of threshold N_f and always for $(\alpha, \beta) = (0.85, 0.05)$ and $N_\nu = \widehat{N}_f = 4096$. The results are summarised in Table 1, whilst Figure 13 shows the comparisons between the curves of Figure 12 and the curves representing the final return loss obtained after applying the algorithm presented above, for $N_f = 1001$, being able to observe well that the curves relating to the final return loss are much narrower than the initial ones and the main lobes are clearly distinguish-

able from each other. As previously ascertained, since the frequency shift estimation is slightly dependent on N_f, assuming the above is also valid in this case, it is appropriate to assume as the most reliable frequency shift, for each value of the glucose concentration (that is, for each case), the one corresponding to $N_f = 1001$ and $(\alpha, \beta) = (0.85, 0.05)$. However, referring to Figure 14, which shows the behaviour of the sample mean and sample standard deviation curves as functions of glucose concentration, derived from the values in Table 1 (e.g., the three values -64.62 MHz, -64.24 MHz, and -65.02 MHz in Table 1, for GC = 100 mg/dL, have $\mu_{shift} \approx -64.63$ MHz and $\sigma_{shift} \approx 0.39$ MHz, as can be appreciated qualitatively in Figure 14), in this case it is possible to note that the values of the sample standard deviation are all "sufficiently" much smaller than the respective values of the sample mean, thence indicating a relatively small dispersion and therefore a high precision, with respect to the N_f variation, for each glucose concentration.

Table 1. Estimated frequency shift, $\overline{f_{shift}}$, for different values of the glucose concentration, GC. The values of the other parameters are: $N_v = 4096$, $\widehat{N}_f = 4096$, $f_{min} = -f_{MAX} = -0.5$ GHz, $(\alpha, \beta) = (0.85, 0.05)$.

	***GC* = 100 mg/dL**	***GC* = 150 mg/dL**	***GC* = 200 mg/dL**	***GC* = 250 mg/dL**	***GC* = 300 mg/dL**
$N_f = 1001$	-64.60 MHz	-56.29 MHz	-49.24 MHz	-42.90 MHz	-38.44 MHz
$N_f = 501$	-64.24 MHz	-55.92 MHz	-49.07 MHz	-42.87 MHz	-38.26 MHz
$N_f = 101$	-65.02 MHz	-56.14 MHz	-48.73 MHz	-43.28 MHz	-39.01 MHz

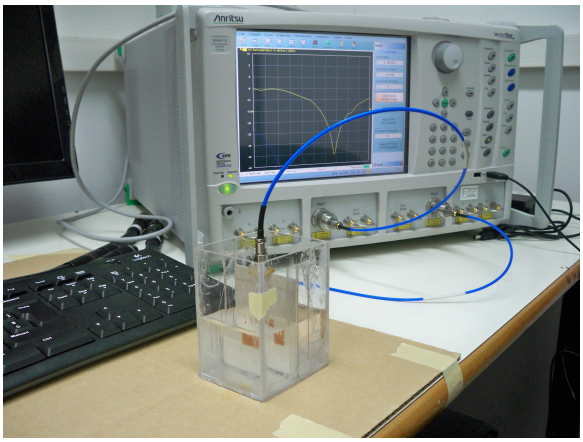

Figure 11. Fabricated microwave sensor and measurement setup at the Microwave Laboratory of University of Calabria.

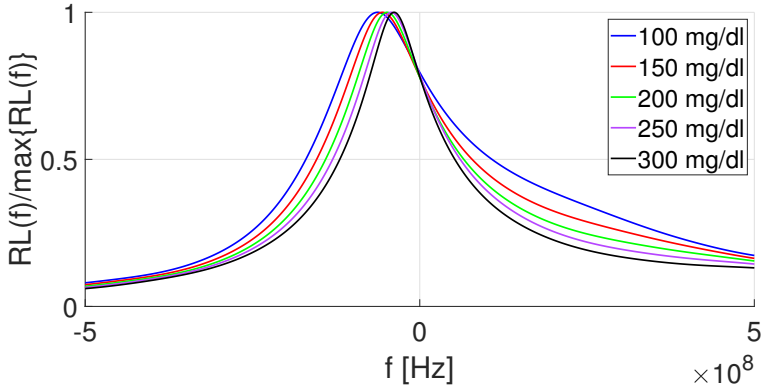

Figure 12. Normalised return loss measured by the patch antenna microwave resonant sensor for different values of the glucose concentration.

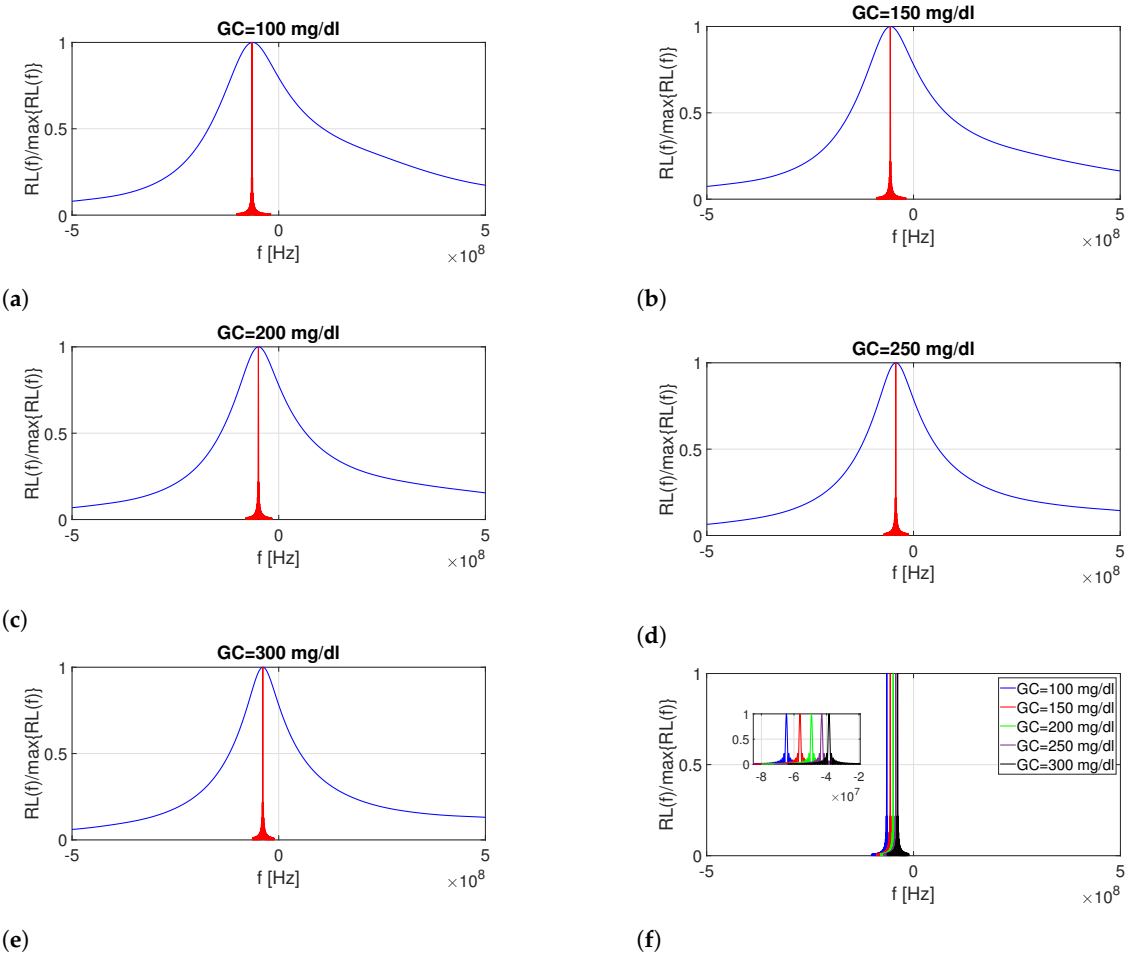

Figure 13. Comparison between the measured normalised return loss (blue curves) and the ones (red curves) returned by applying the proposed algorithm (**a**–**e**). (**f**) Shows the comparison between the red curves of (**a**–**e**). The parameters were set as follows: $N_f = 1001$, $N_\nu = \widehat{N}_f = 4096$, $(\alpha, \beta) = (0.85, 0.05)$.

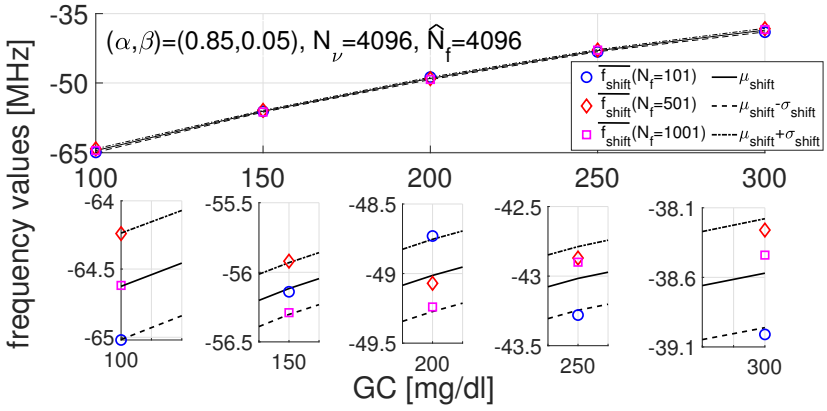

Figure 14. Estimated frequency shift, $\overline{f_{shift}}$, sample mean, μ_{shift}, and sample standard deviation, σ_{shift}, of $\overline{f_{shift}}$ as functions of the glucose concentration (GC), for $N_f = 101,\ 501,\ 1001$.

5. Conclusions

In this work, an iterative algorithm was presented by which to significantly increase the resolution of resonant microwave sensors, in such a way as to be able to track the shift of the resonance frequency with great accuracy. A test procedure was first carried out on synthetic signals, generated *ad hoc*, in order to highlight its peculiar characteristics. Subsequently, the algorithm was successfully applied to a simplified scenario related to the

problem of blood glucose monitoring. The above algorithm revealed a high flexibility from the implementation point of view, and the achieved results proved to be satisfactory. More complex test scenarios will be considered in future works.

Author Contributions: Conceptualisation, R.S. and G.B.; methodology, R.S. and G.B.; software, G.B.; validation, G.B.; formal analysis, G.B.; investigation, G.B.; resources, R.S. and S.C.; data curation, A.B. and G.B.; writing—original draft preparation, G.B.; writing—review and editing, S.C. and R.S.; visualisation, G.B.; supervision, A.B., S.C., and R.S.; project administration, S.C. and R.S.; funding acquisition, S.C. and R.S. All authors have read and agreed to the published version of the manuscript.

Funding: This research was funded by MIUR (Ministero dell'Istruzione dell'Università e della Ricerca), Italy, under project grant PRIN 2017 "Microwave Biosensors: Enhanced Non-Invasive Methodology for Blood Glucose Monitoring".

Data Availability Statement: The data presented in this study are available on request from the corresponding author.

Conflicts of Interest: The authors declare no conflict of interest. The funders had no role in the design of the study; in the collection, analyses, or interpretation of data; in the writing of the manuscript, or in the decision to publish the results.

Abbreviations

DTFT	Discrete-Time Fourier Transform
PE	Percentage Error
BW	Beam-Width
GC	Glucose Concentration

References

1. Martín, F.; Vélez, P.; Gil, M. Microwave Sensors Based on Resonant Elements. *Sensors* **2020**, *20*, 3375. [CrossRef] [PubMed]
2. Costanzo, S. Non-invasive microwave sensors for biomedical applications: New design perspectives. *Radioengineering* **2017**, *26*, 406–410. [CrossRef]
3. Costanzo, S. Loss tangent effect on the accurate design of microwave sensors for blood glucose monitoring. In Proceedings of the 11th European Conference on Antennas and Propagation EuCAP, Paris, France, 19–24 March 2017.
4. Omer, A.E.; Shaker, G.; Safavi-Naeini, S. Portable Radar-Driven Microwave Sensor for Intermittent Glucose Levels Monitoring. *IEEE Sens. Lett.* **2020**, *4*, 1–4. [CrossRef]
5. Grenier, K.; Dubuc, D.; Chretiennot, T.; Chen, T.; Artis, F.; Poupot, M.; Fournié, J.J. Noncontact measurement of complex permittivity and thickness by using planar resonators. *IEEE Trans. Microw. Theory Tech.* **2015**, *64*, 247–257.
6. Ong, K.; Grimes, C.; Robbins, C.; Singh, R. Design, and application of a wireless, passive, resonant-circuit environmental monitoring sensor. *Sens. Actuators A Phys.* **2001**, *93*, 33–43. [CrossRef]
7. Gil, M.; Vélez, P.; Aznar-Ballesta, F.; Muñoz-Enano, J.; Martín, F. Differential sensor based on electroinductive wave transmission lines for dielectric constant measurements and defect detection. *IEEE Trans. Antennas Propag.* **2020**, *68*, 1876–1886. [CrossRef]
8. Mata-Contreras, J.; Herrojo, C.; Martin, F. Application of split ring resonator (SRR) loaded transmission lines to the design of angular displacement and velocity sensors for space applications. *IEEE Trans. Microw. Theory Tech.* **2017**, *65*, 4450–4460. [CrossRef]
9. Zarifi, M.H.; Sohrabi, A.; Shaibani, P.M.; Daneshmand, M.; Thundat, T. Detection of volatile organic compounds using microwave sensors. *IEEE Sens. J.* **2015**, *15*, 248–254. [CrossRef]
10. Chretiennot, T.; Dubuc, D.; Grenier, K. A microwave and microfluidic planar resonator for efficient and accurate complex permittivity characterization of aqueous solutions. *IEEE Trans. Microw. Theory Tech.* **2012**, *61*, 972–978. [CrossRef]
11. Abbasi, Z.; Baghelani, M.; M. Daneshmand, M. High-Resolution Chipless Tag RF Sensor. *IEEE Trans. Microw. Theory Tech.* **2020**, *68*, 4855–4864. [CrossRef]
12. Abbasi, Z.; Daneshmand, M. Contactless pH measurement based on high resolution enhanced Q microwave resonator. In Proceedings of the 2018 IEEE/MTT-S International Microwave Symposium-IMS, Philadelphia, PA, USA, 10–15 June 2018; pp. 1156–1159.
13. Gerchberg, R.W. Super-resolution through error energy reduction. *Opt. Acta* **1974**, *21*, 709–720. [CrossRef]
14. Papoulis, A. A New Algorithm in Spectral Analysis and Band-Limited Extrapolation. *IEEE Trans. Circuits Syst.* **1975**, *22*, 735–742. [CrossRef]
15. Pozar, D. *Microwave and RF Design of Wireless Systems*; John Wiley & Sons, Inc.: New York, NY, USA, 2000; p. 34.
16. Childers, D.G.; Skinner, D.P.; Kemerait, R.C. The Cepstrum: A Guide to Processing. *Proc. IEEE* **1977**, *65*, 1428–1443. [CrossRef]
17. MATLAB. Available online: https://www.mathworks.com/ (accessed on 31 October 2021).

18. Costanzo, S.; Cioffi, V.; Lopez, G. Tissue-Mimicking Phantoms: Dielectric Characterization and Design of a Multi-layer Substrate for Microwave Blood Glucose Monitoring. *Adv. Intell. Syst. Comput.* **2021**, 223–239. [CrossRef]
19. Dima, R.; Buonanno, G.; Solimene, R. Comparing two fitting algorithms for determining the Cole-Cole parameters in blood glucose problems. In Proceedings of the 2nd International Electronic Conference on Applied Sciences Session, Online, 15–31 October 2021.